

The Spatial Distributions of Radiation Emitted from a Sinusoidal Current Filament and a Dipole Antenna

Edmund K. Miller

Los Alamos National Laboratory (Retired)
e.miller@ieee.org

Abstract – While the analytical and numerical tools for determining the basic properties of a variety of antenna types have been long-established, there remains some continuing curiosity about how electromagnetic radiation is launched by such a simple antenna as a dipole. The following article discusses this problem in both the frequency domain and time domain. The sinusoidal current filament (SCF) is investigated first as a prototype of a wire dipole. The length-wise distribution of radiated power for the SCF is obtained from the distributed radiation resistance of Schelkunoff and Feldman, the induced electromotive force (IEMF) method, and the far-field analysis of radiation sources (FARS) developed by the author.

The FARS approach is next used to analyze a frequency-domain numerical model of a dipole antenna, producing results similar to those for the SCF for a dipole of near-zero radius. Differentiating the decaying on-surface Poynting vector (PV) produces results comparable to those from FARS to explicitly demonstrate the power loss caused by radiation of the propagating current and charge. The lobed distributed radiated power is shown to be closely correlated with the square of the dipole current, confirming the cause of the radiation to be due to a partially reflected charge as the current and charge form standing waves on the dipole. Application of a time-domain version of FARS yields a smoothed length-wise distribution of radiated energy as opposed to the lobed variation of the frequency domain.

Index Terms – Charge reflection, dipole radiation, differentiated Poynting vector (DPV), distributed radiation resistance, far-field analysis of radiation sources, IEMF method, NEC, Poynting vector, sinusoidal current filament, TWTD.

I. INTRODUCTION

How electromagnetic fields are radiated from such a simple antenna as a wire dipole seems to have been periodically revisited over the years. Perhaps, the first discussion related to this problem is due to Poynting who introduced the concept of electromagnetic power

flow with a vector that bears his name. Streamline plots of Poynting vectors (PVs) near a dipole reveal the flow of power from the feedpoint along the antenna where they successively leave the antenna to become far-field radiation [1]. Computation of the power flow along the antenna exhibits a monotonic decrease down the arms of the dipole to its ends where the charge is reflected and the current becomes zero.

While the PV streamlines reveal a tantalizing image of power flow extending from the antenna feedpoint to the far field, their interpretation can be misleading. If the streamlines are constructed such that each represents the same amount of power flow, each will reach a different point on the far-field sphere with their angular separation dependent on the radiation pattern. Tracing them back to the dipole itself, each seems to bend away from it along its length at a different location. This might be interpreted to mean that a given angular steradian on the far-field sphere receives its power solely from a particular and different area of the antenna.

But numerical evaluation of the electric and magnetic fields around the antenna at any specific angle and distance involves integrating over its entire surface. This implies, to the contrary, that the charge and current distribution over the entire antenna potentially have some effect on the radiation at any given location in the far field. These two observations cannot both be true. Thus, some other interpretation is needed to establish the quantitative origin of where and how radiated power originates from over the antenna. The purpose of the following discussion is to provide some different ways of doing so. Two different but related kinds of radiating sources are considered: the sinusoidal current filament (SCF) and a dipole antenna consisting of a perfect electric conductor (PEC). This paper is motivated in part by a recent article by Jackson [1] who referred to the radiation emitted by a dipole antenna saying it somehow “ultimately shakes free” as the current propagates down its length.

The following discussion provides physical and computational demonstrations for how, why, and where the radiated power leaves, or shakes free, from the

dipole. This is done using various analytical procedures to determine the radiated-power density on a per-unit-length basis. The dipole results are obtained using Numerical Electromagnetics Code (NEC) [2], a well-validated computer model based on the thin-wire electric-field integral equation solved using the method of moments [3]. The moment method, widely used in the engineering electromagnetics community, involves sampling an unknown source such as a current distribution using basis functions and sampling boundary conditions using testing functions. While this procedure is representative of any electromagnetic numerical model, whether formulated using the differential or integral forms of Maxwell's equations, it has come to be typically associated with an integral-equation formulation.

While modeling linear objects such as wires, 6-10 samples per wavelength usually provide acceptably accurate results, the numerical results that follow use 20 samples per wavelength. This higher sampling rate is used for both the SCF and NEC dipole to ensure an acceptable accuracy for the far-field results and for their numerical comparisons. Note that the spatial density of the emitted radiated power in the frequency domain (FD) or radiated energy in the time domain (TD) can be expressed in two ways. One is on a per wavelength basis (FD) or on a per segment basis for either domain. The total power or energy can conveniently be normalized to 1 W or 1 J, respectively.

II. THE SINUSOIDAL CURRENT FILAMENT

The SCF has served as a surrogate for a wire antenna in the pre-computer era. It has the advantage of having closed-form expressions for its near and far fields and it closely approximates the current on an actual PEC thin-wire dipole. In a 1942 article [4], Schelkunoff and Feldman introduced the concept of a distributed radiation resistance, $R_{rad,SF}(x)$. Their analysis used the SCF as an analytical model

$$I(x) = I_0 \sin[k(L - |x|)], \quad -L \leq x \leq L, \quad (1)$$

while conducting experimental measurements to confirm their results using a wire antenna. They derived an expression for $R_{rad,SF}$ given by

$$R_{rad,SF}(x) = \frac{60L}{L^2 - x^2}, \quad (2)$$

where they restricted the length $2L$ of the antenna to an integral number of half-wavelengths and the feedpoint is at a current antinode. Further examination of their work [3] shows that eqn (1) can be generalized to

$$R_{rad,SF}(x) = 30 \frac{1}{\sin \beta(L - |x|)} \left[\frac{\sin \beta(L - x)}{L - x} - 2 \frac{\sin \beta x}{x} \cos \beta L + \frac{\sin \beta(L + x)}{L + x} \right]. \quad (3)$$

The radiated-power density is then given by

$$p_{rad}(x) = \frac{1}{2} I^2(x) R_{rad,SF}(x) = 15I(x) \left[\frac{\sin \beta(L - x)}{L - x} - 2 \frac{\sin \beta x}{x} \cos \beta L + \frac{\sin \beta(L + x)}{L + x} \right]. \quad (4a)$$

In the following discussion, both the SCF and wire dipoles are divided into N equal-length segments for numerical purposes using the method of moments [3]. The radiated power per segment of an SCF having N segments of length $2L/N$ is then

$$p_{rad/seg}(x_i) = \frac{1}{2} I^2(x_i) R_{rad,SF}(x_i) \Delta x, \quad (4b)$$

where Δx is the segment length. This expression provides a useful confirmation for two other methods described below to obtain the spatial distribution of power radiated by the SCF.

The SCF distributed radiation resistance $R_{rad,SF}(x)$ from eqn (3) varies with its length L due to the slope discontinuity in the current that can occur at the origin $x = 0$. The SCF current in the range $-1 \leq x \leq +1$ for $L = 10l/2$ or $5.0l$ wavelengths and $L = 11l/2$ or 5.5 wavelengths is plotted in Figure 1 with $N = 101$ and 111 segments, respectively. This value of N was used to produce a symmetric distribution about the origin. The current slope at the origin for $L = 5.0$ has a sharp discontinuity at the origin, while for $L = 5.5$, there is no slope discontinuity. The distributed radiation resistances for these two cases are plotted in Figure 2. The 5-wavelength SCF becomes infinite at the origin, a point necessarily omitted in the plot. The 5.5-wavelength SCF, on the other hand, exhibits a smooth minimum there.

The radiated-power density from eqn(4) is plotted in Figure 3 where a striking difference is seen between the two SCF lengths. The current-slope discontinuity at the origin for the 5-wavelength case and the corresponding peak it causes in the $R_{rad,SF}(x)$ results in a sharp doublet in the radiated-power distribution. This doublet in

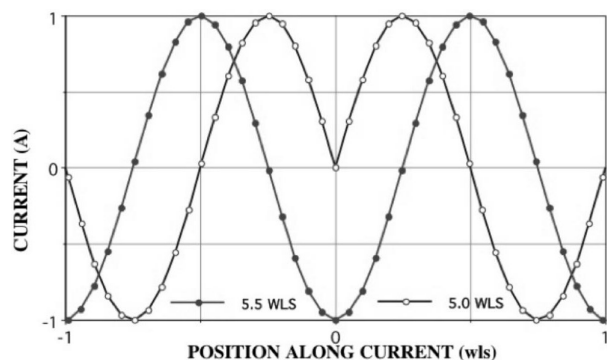


Fig. 1. The center portions of sinusoidal current filaments an even and odd number of half wavelengths long.

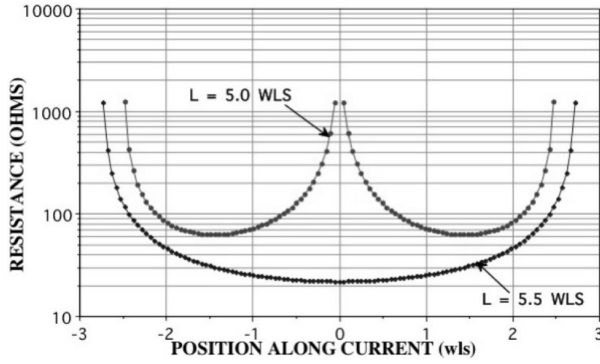


Fig. 2. The distributed radiation resistances from Schelkunoff and Feldman of sinusoidal current filaments an even and odd number of half wavelengths long.

radiated power is due to charge-density maxima caused by the current-slope discontinuity at the origin. Similar but smaller effects occur for other SCF lengths while becoming zero only when n is an odd integer. The lobed structure of the radiated power will be explained after results for a dipole antenna are also presented.

Another way to determine the radiated-power distribution for the SCF is the induced electromotive force (IEMF) method. The IEMF method involves using the tangential electric field $E_x(x)$ along the SCF as given by

$$E_x(x) = \frac{j\eta_0 I_0 e^{-jkr}}{4\pi k\rho r} \left\{ k \cos(kx) - (1 + jkr) \frac{(x-x)^2}{r^2} [\sin(kx)] \right\}_{x=-L}^{x=L}. \quad (5)$$

Having the field along each current segment the associated supplied power for segment i can then be obtained from

$$P_{\text{IEMF/seg}}(x_i) = \frac{1}{2} \int_{\Delta x_i} I(x) \text{Re}[E_x(x)] dx \approx \frac{1}{2} I(x_i) \text{Re}[E_x(x_i)] \Delta x. \quad (6)$$

Note that the IEMF result is an input quantity and so is opposite in sign to a positive radiated power. For comparison purposes here, however, the IEMF results are plotted as a positive quantity.

The IEMF power results from eqn (6) for the 5.0- and 5.5-wavelength SCFs are compared with the $R_{\text{rad,SF}}(x)$ results of Figures 3 and 4 where they can be seen to be graphically indistinguishable. Concerning this agreement, it is worth noting that eqn (5) can be written as

$$P_{\text{rad/seg}}(x_i) = \frac{1}{2} I^2(x_i) R_{\text{rad,SF}}(x_i) \Delta x = -\frac{1}{2} I(x_i) E_x(x_i) \Delta x \approx -P_{\text{IEMF/seg}}(x_i) \quad (7)$$

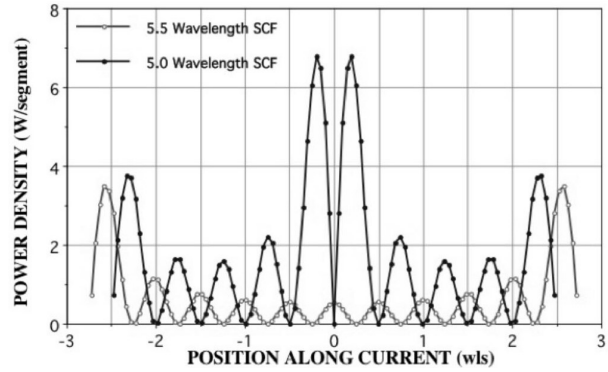


Fig. 3. The distributed radiated-power densities per segment for sinusoidal current filaments an even and odd number of half wavelengths long from eqn (5).

and that the two methods are essentially equivalent. This result confirms the validity of the distributed radiation-resistance concept of Schelkunoff and Feldman.

An alternate approach to evaluating the radiated-power distribution of the SCF is far-field analysis of radiation sources (FARS) [4]. As its name implies, FARS is based on the far field that for the SCF can be written as [5]

$$E_{\text{rad},\theta}(\theta) = j\eta_0 \frac{I_0 e^{-jkr}}{2\pi r} \left[\frac{\cos(kL \cos \theta) - \cos(kL)}{\sin \theta} \right], \quad (8a)$$

or

$$E_{\text{rad},\theta}(\vartheta) = j\eta_0 \frac{I_0 e^{-jkr}}{2\pi r} \frac{1}{\sin(\theta)} \left[e^{(j k L) \cos(\theta)} + e^{-(j k L) \cos(\theta)} - 2 \cos(kL) \right] \quad (8b)$$

where $E_{\text{rad},\theta}$ is the θ component of the electric field. Note that the bracketed terms in eqn (8b) have the appearance of three point sources located at the ends and center of the SCF. This has led to speculation that the SCF radiates from only those three locations, but this is not the case as shown by Figure 3 and elsewhere [6] due to the $\sin(\theta)$ in the denominator of eqn (8).

The implementation of FARS involves evaluating the far radiated field in a slightly modified way compared to the usual computation of the radiated power from some object. This is done by developing the far-field power on an incremental basis in the context of the moment method. The incremental FARS power, $p_{i,\text{FARS}}(\theta, \varphi)$ for segment s_i in observation direction θ, φ is

$$p_{i,\text{FARS}}(\theta, \varphi) = \lim_{r \rightarrow \infty} \left(r^2 \frac{1}{2\eta} \text{Re}[e_i(\theta, \varphi) \cdot E^*(\theta, \varphi)] \right) \quad (9)$$

where $\vec{e}_i(\theta, \varphi)$ is the electric field due to source (or segment) i and η is the medium impedance while the total electric field for N sources or segments, denoted by

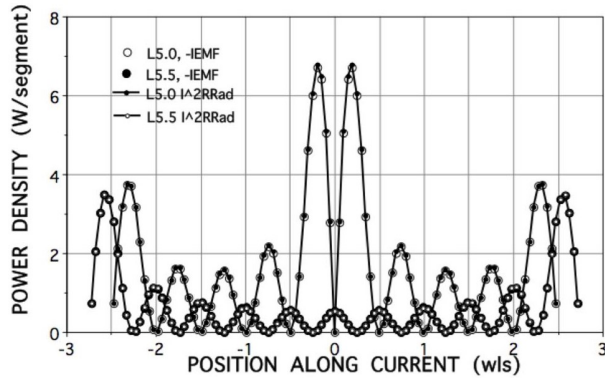


Fig. 4. The $I^2(x)R_{rad,SF}(x)$ and IEMF distributed radiated-power densities for sinusoidal current filaments an even and odd number of half wavelengths long.

$E(\theta, \varphi)$, is

$$E(\theta, \varphi) = \sum_1^N e_i(\theta, \varphi). \quad (10)$$

The total power contributed by segment i , denoted as $P_{i,FARS}$, comes from integrating the incremental result $p_{i,FARS}(\theta, \varphi)$ over all θ, φ to obtain

$$P_{i,FARS} = \int_0^\pi \int_0^{2\pi} p_{i,FARS}(\theta, \varphi) \sin\theta d\theta d\varphi, \quad (11)$$

as the total power coming from segment i .

Finally, the total radiated power is obtained from integrating the $P_{i,FARS}$ samples over all N sources, or

$$P_{FARS} = \sum_1^N P_{i,FARS}. \quad (12)$$

Note that the FARS computation differs from a conventional evaluation of the total far-field power only in defining the intermediate quantity $P_{i,FARS}$, the individual contribution of each incremental source, to the total radiated or scattered power. Note also that there is no constraint that each $P_{i,FARS}$ be positive, with a negative value indicating that a particular segment is reducing the total radiated power.

III. THE NEC DIPOLE

Next considered is a comparison of FARS results for the SCF and an NEC-modeled dipole antenna presented in Figure 6. The NEC radiated power is slightly less than that for the SCF since the NEC current decays in amplitude away from the feedpoint.

The normalized, on-surface real component of the PV for a 10-wavelength NEC dipole is shown in Figure 7, as computed from the conjugate product of the wire charge density and current divided by 2. A longer dipole is used here to exhibit more clearly the decay in power flow along the dipole due to radiation. Power flow to the right is shown as positive and to the left is shown as negative in this graph. The normalized complex current

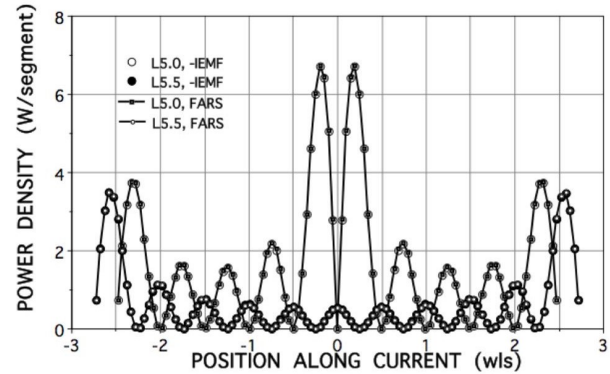


Fig. 5. The IEMF and FARS distributed radiated-power densities for sinusoidal current filaments an even and odd number of half wavelengths long.

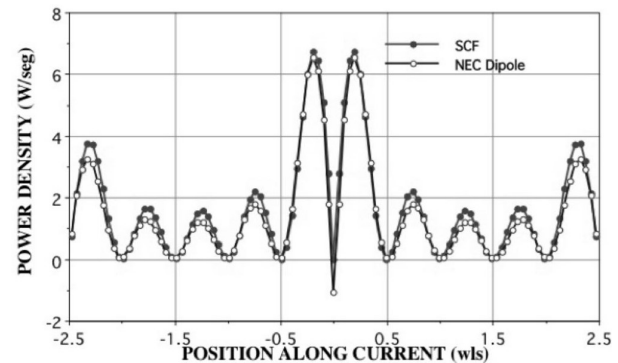


Fig. 6. A comparison of the FARS radiated-power density for a 1-A, 5-wavelength sinusoidal current filament, and an NEC dipole having a current maxima of 1 A.

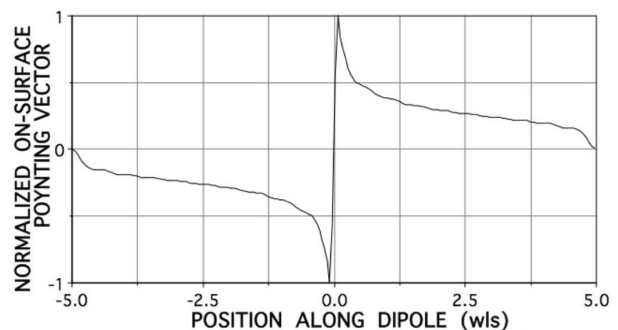


Fig. 7. The normalized on-surface Poynting vector $PV_{jj}(x)$ along a center-fed, 10-wavelength dipole.

on the dipole is plotted in Figure 8 where the real part decays substantially more than the quadrature, or imaginary, component.

There is a slight oscillation in the PV of Figure 7, the effect of which is emphasized by differentiating it to pro-

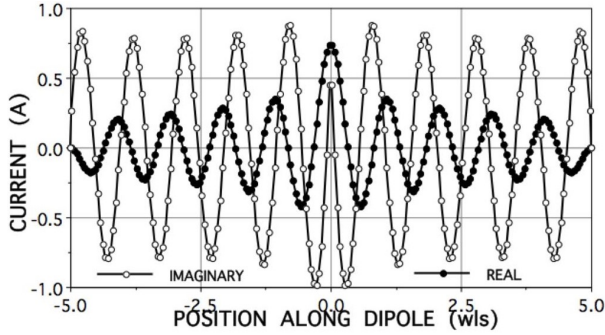


Fig. 8. The normalized complex current on a 10-wavelength dipole antenna.

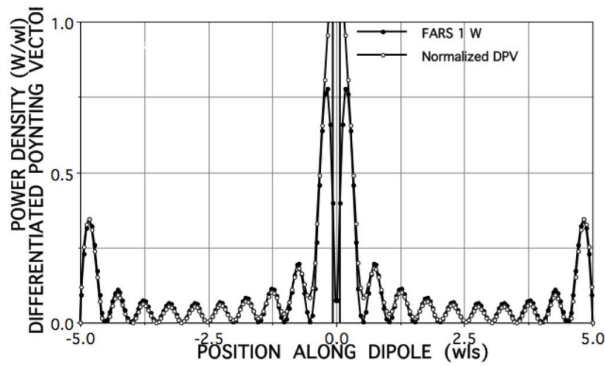


Fig. 9. Normalized DPV and FARS radiated-power densities for a 10-wavelength, center-fed dipole.

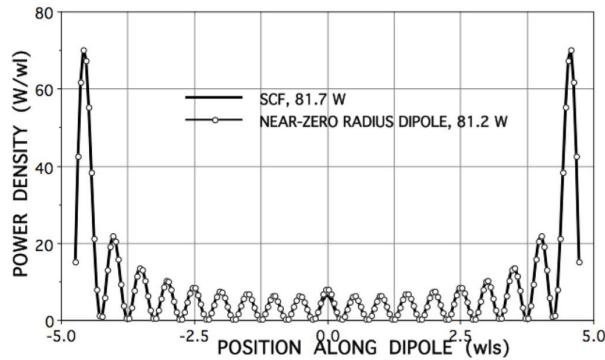


Fig. 10. FARS power densities for a 9.5-wavelength SCF and NEC dipole with maximum currents of 1 A.

duce the loss rate of radiated power with distance from the feedpoint as presented in Figure 9. Also included for comparison is the FARS radiated-power density, with the end maxima of the differentiated PV (DPV) normalized to the FARS result. Observe that the FARS result, being based entirely on the far field, does not explicitly include the effect of the input power provided by the exciting voltage at the antenna feedpoint as does the

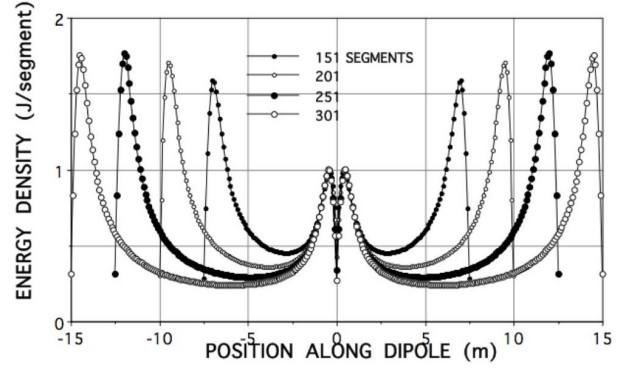


Fig. 11. The energy densities of dipoles of 151-301 0.1-m long segments excited by a Gaussian voltage pulse.

IEMF method. The agreement between the two methods for determining the quantitative absolute (FARS) or relative (DPV) radiated-power distribution is within a few percent, providing mutual validation for both.

FARS results for an NEC dipole of decreasing radius were obtained for comparison with an SCF [3]. The NEC results converged to within 1% of the SCF values for a dipole radius of 10^{-20} wavelengths.

FARS has also been implemented in the TD [7, 8] using the computer model thin-wire time domain (TWTD) [9]. A result for several dipoles of different lengths with center feedpoints is presented in Figure 11 where the excitation is a Gaussian pulse with a half-amplitude width of about 13 time steps, Δt , and with the segment length $\Delta x = c\Delta t$. The energy density is a smooth function of position in contrast with the frequency-domain result.

A comparison of a 10-m center-fed dipole radiating 1 J in the TD, a normalized version of the 101-segment curve of Figure 11, and a 10-wavelength dipole radiating 1-W in the FD is shown in Figure 12. The standing-wave nature of the frequency-domain dipole presents a distinctive contrast compared with the time-domain result.

IV. ACCELERATED CHARGE AND RADIATION

Three methods for determining where and how much radiation originates from an SCF have been presented above: the Schelkunoff-Feldman radiation resistance, a closely related procedure, the IEMF method, and FARS. Two, the DPV and FARS, have been shown to provide the same kind of information for a PEC dipole. Since charge acceleration is known to be the cause for electromagnetic radiation, the question remains about where and why does this occur on a PEC object? The answer to this question for an SCF is clear: Being a purely standing wave with zero net power propagation along its length, charge is accelerated due to an applied

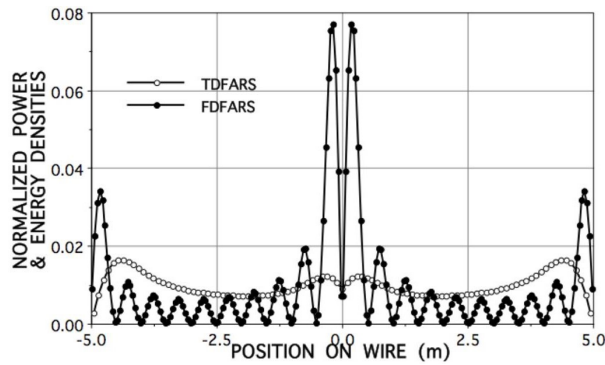


Fig. 12. Comparison of frequency-domain and time-domain FARS for a 10-m center-fed dipole radiating a total power of 1 W or energy of 1 J, respectively.

electric field as demonstrated by the IEMF method, with the result corroborated by FARS.

Where charge acceleration occurs on a PEC needs some further discussion. It is clear that charge is set into motion, or accelerated, at the feedpoint where an exciting electric field is applied. In addition, the current goes to zero at the ends of a finite-length antenna where the charge is completely reflected and is thus consequently accelerated, as well. But both the frequency-domain and time-domain versions of FARS show that radiation and accompanying charge acceleration must occur all along the interior length of a dipole. So the question to be considered is what is the cause of this interior acceleration.

A related phenomenon provides the answer. It has been observed that the current propagating down a wire of constant radius decays in amplitude, with the cause being attributed to power loss due to radiation. This result of this decay is exhibited by the on-surface PV in Figure 7 where the power flow decays in an oscillatory but monotonic fashion with increasing distance from the feedpoint. Because charge is conserved, the conclusion follows that some portion of the outward-propagating charge and current is reflected back toward the feedpoint. This reflection and associated charge acceleration thus account for the radiation that takes place down the arms of the dipole antenna.

This raises the additional question about what causes the charge reflection itself to occur. It is known that the total current on an infinite biconical antenna is independent of distance from the feedpoint [5], i.e., there is no reflection because the bicone wave impedance is independent of position. An infinite wire or cylinder of constant radius by contrast has a variable, distance-dependent, wave impedance and so a partial reflection of a propagating current occurs. This accounts for what can be described as “propagation radiation” as shown by the FARS results in Figures 9 and 10

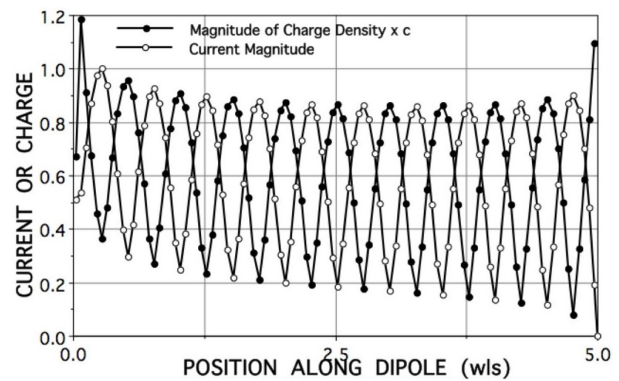


Fig. 13. The magnitudes of the standing-wave current and charge distributions on half of a 10-wavelength, center-fed dipole antenna.

where radiation lobes occur at half-wavelength intervals. On the other hand, for a dipole antenna excited by a short-pulse electric field, there is no standing wave. Instead, the propagation radiation is a smooth, continuous curve extending between the feedpoint and wire ends as shown in Figures 11 and 12 as obtained using TWTD [9].

The cause of the lobed, standing-wave radiation power in the FD is simply explained. The counter-propagating sine waves of current and charge produce standing waves of the kind shown for one-half of a 10-wavelength dipole in Figure 13. The peaks and minima of the current and charge magnitudes are interleaved. The plot of the FARS radiated-power density and the square of the normalized current in Figure 14 shows that their lobe maxima are aligned. This is because current maxima are produced when opposite-signed, counter-propagating charge waves meet. The partial reflection of opposite-signed charges moving in opposite directions produces additive radiated electric fields, resulting in the FARS maxima. Charge maxima, on the other hand, occur when same-signed charge waves meet. Their partial reflections produce canceling radiated electric fields that result in FARS minima. These results demonstrate why and where the radiation originates from the PEC dipole.

Observe that the effective propagation speed of the current and charge waves on the PEC wire is approximately at the speed of light in the medium in which the dipole is located, a fact that deserves some additional discussion. Observe that when modeling in the TD, charge and current pulses are found to move at approximately the speed of light along a uniform-radius, straight wire. However, this phenomenon does not require any physical charge to move at near-light speed. Instead, it arises from the fact that the fields launched from the feedpoint

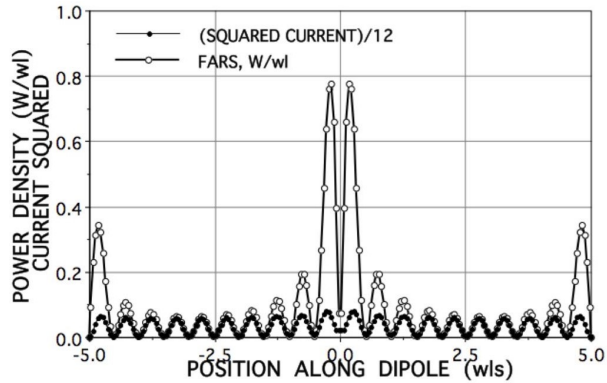


Fig. 14. The FARS power density in W/wavelength for a 10-wavelength, center-fed dipole together with the square of the current normalized to the inner FARS lobes.

of an impulsively excited wire propagate along the wire near or at the speed of light of the medium in which the wire is located. The magnetic and electric fields associated with these pulses must terminate on the wire as required by the boundary conditions of a PEC. This process can be analogized in various ways [9] or as a row of falling dominos. Each domino moves very little but with the overall effect propagating along the entire row.

Since the tangential electric field on the wire surface is zero, there is only a radial field that terminates at the charge on its surface. Similarly, since the normal magnetic field on the wire surface is zero, there is only a tangential, or azimuthal, magnetic field that terminates at the current on its surface. Thus, the moving charge and its accompanying current are attached to the propagating fields. When the field propagation is interrupted by ends, bends, loads, junctions, etc., some or all of the propagating fields and Q/I pulses are reflected with the reflected field lines developing bends as discussed in Chapter 2.

While the magnetic field lines are closed around a wire antenna since there is no magnetic charge, the radiated electric fields from finite objects must eventually form closed lines as well to “break off” from it. This is easily visualized for an impulsively excited object in the TD. After enough time has passed, the object must return to overall charge neutrality which means that there are no remaining electric or magnetic fields attached to its surface. Closure of the electric fields occurs when opposite-signed charges can neutralize each other as they pass moving in opposite directions.

It is reasonable to ask whether the equivalent sources used in boundary-value problems match physical reality, i.e., whether their computed results match measurements. The computed radiated fields have been found to match the measured radiation and scattering patterns within their respective numerical and experimental uncertainties since the beginning of electromagnet-

ics as a discipline. Measurements of near-field interactions and input impedance are somewhat more experimentally difficult to determine, but they also have confirmed analytical and computational results. One of the more demanding checks on computations is measurement of the source distribution on an object. Examples of frequency-domain measurements for current distributions can be found in the literature such as 10–15.

REFERENCES

- [1] J. D. Jackson, “How an antenna launches its input power into radiation: the pattern of the Poynting vector at and near an antenna,” *American Journal of Physics*, vol. 74, no. 4, pp. 280-288, 2006.
- [2] S. A. Schelkunoff and C. B. Feldman, “On radiation from antennas,” *Proceedings of the I.R.E.*, pp. 511-516, Nov. 1942.
- [3] E. K. Miller, “Comparison of the radiation properties of a sinusoidal current filament and a PEC dipole of near-zero radius,” *IEEE Antennas and Propagation Society Magazine*, vol. 48, no. 4, pp. 37-47, Aug. 2006.
- [4] E. K. Miller, “PCs for AP and other EM reflections,” *IEEE AP-S Magazine*, vol. 41, no. 2, pp. 82-86, Apr. 1999a; vol. 41, no. 3, pp. 83-88, Jun. 1999b.
- [5] C. A. Balanis, *Antenna Theory*, Harper & Row, New York, 1982, pp. 118-124.
- [6] E. K. Miller, “The incremental far field and degrees of freedom of the sinusoidal current filament,” *IEEE Antennas and Propagation Society Magazine*, vol. 49, no. 4, pp. 13-21, Aug. 2007.
- [7] E. K. Miller and G. J. Burke, “A multi-perspective examination of the physics of electromagnetic radiation,” *Applied Computational Electromagnetics Society (ACES) Journal*, vol. 16, no. 3, pp. 190-201, 2001.
- [8] E. K. Miller, “Time-domain far-field analysis of radiation sources,” *IEEE Antennas and Propagation Society Magazine*, vol. 53, no. 5, pp. 81-97, Oct. 2011.
- [9] E. K. Miller, “Exploring electromagnetic physics using thin-wire time-domain (TWT) modeling,” *Proceedings of 14th Annual Review of Progress in Applied Computational Electromagnetics*, Naval Postgraduate School, Monterey, CA, pp. 583-588, 1998.
- [10] C. S. Baird, “What is the speed of electricity,” *Science Questions with Surprising Answers*, Feb. 19, 2014.
- [11] R. W. P. King and T. T. Wu, “Current measurement-1965-currents, charges, and near fields of cylindrical antennas,” *Radio Science*, vol. 69D, no. 3, pp. 429-446, 1965.

- [12] W. D. Smith, "Numerical analysis of normal mode helical dipoles antennas," PhD Dissertation, Iowa State University, 1971.
- [13] T. Yokoyama, T. Hoashi, K. Murata, S. Egashira, K. Egashira, and T. Nakamiya,, "Design of multi-band antenna using different radius wires," *PIERS Online*, vol. 5, no. 3, 2009.
- [14] T. Ishizone, S. Adachi, K. Taira, Y. Mushiake, K. Mitazaki, "Measurement of antenna current distribution in an anisotropic plasma," *IEEE Transactions on Antennas and Propagation*, pp. 678-679, Sep. 1969.
- [15] S. Egashira, M. Taguchi, and A. Sakitani, "Consideration on the measurement of current distribution on bent wire antennas," *IEEE Transactions on Antennas and Propagation*, vol. 36, no. 7, pp. 918-926, Jul. 1988.
- [16] Y. S. H. Khraisat and K. A. Hmood, "Distribution of symmetrical dual and triple feeding full-wave dipole antenna," *Modern Applied Science*, vol. 5, no. 6, pp. 126-132, Dec. 2011.



Edmund K. Miller received the Ph.D. degree in electrical engineering from the University of Michigan in 1965 with an emphasis on computational electromagnetics (CEM), a rapidly developing field at the time.

His working career has been quite varied including employment at four universities

(Michigan Technological University, University of Michigan, Kansas University, and Ohio University), three companies (MBAAssociates, Rockwell International Science Center, and General Research Corporation, all in California), and two national laboratories (Lawrence Livermore and Los Alamos from which he retired in 1993). He has served two terms on the IEEE Antennas and Propagation Society (AP-S) Administrative Committee and has twice been an APS Distinguished Lecturer.

Dr. Miller was elected as IEEE Fellow in 1984 and received the IEEE Third Millennium Medal in 2000. He was the recipient (with others) of the 1988 Best Paper Award from the IEEE Education Society. Between 1985 and 2002, he served on the editorial board of IEEE Potentials Magazine as Editor or Associate Editor for which he wrote a regular column "On The Job." He also wrote a column for the AP-S Magazine "PCs for AP and Other EM Reflections" from 1984 to 2000. He was an organizer, served as its first president, and is a Fellow of the Applied Computational Electromagnetics Society (ACES) for which he served two terms on its Board of Directors. His research interests include CEM, applied signal processing, visual electromagnetics, and promoting the incorporation of accuracy statements in published CEM numerical results. He has published numerous articles dealing with his major interest, the physics of electromagnetic radiation, and recently completed a draft book on the topic with the title "Charge Acceleration and the Spatial Distribution of Radiation Emitted by Antennas and Scatterers."